J Mater Sci (2015) 50:8166–8174
DOI 10.1007/s10853-015-9395-0

In-plane mechanical properties of carbon nanotube films fabricated by floating catalyst chemical vapor decomposition

Fujun Xu[1] · Baochun Wei[1] · Wei Liu[2] · Hongfei Zhu[1] · Yongyi Zhang[3] · Yiping Qiu[1]

Received: 15 June 2015 / Accepted: 27 August 2015 / Published online: 3 September 2015

Abstract Large-scale carbon nanotube (CNT) films fabricated by floating catalyst chemical vapor deposition (FCCVD) are promising reinforcement materials for high performance composites. However, little research has been reported on the four independent in-plane engineering constants of FCCVD CNT films, which are essential for understanding and prediction of mechanical behavior of FCCVD CNT film-based structures. The tensile strength in CNT-oriented direction is 127 MPa and the tensile modulus in oriented and transverse directions are 3.0 and 0.3 GPa, respectively. These mechanical properties are mainly attributed to the as-grown CNT-to-CNT contacts in the films. The Poisson's ratio in the oriented direction at 5 % strain is 0.75. A negative Poisson's ratio of −0.99 is observed at 0.1 % strain in CNT-oriented direction. The in-plane shear modulus is 0.57 GPa, which is derived from the coordinate transformation between the on-axis and 45° off-axis compliance matrices. The in-situ scanning electron microscopy is adopted to observe the microstructure at different tensile strains. During the tensile testing, the reorientation of CNT bundles in CNT film is evaluated by numerical image processing and Raman spectroscopy.

✉ Yiping Qiu
ypqiu@dhu.edu.cn

Fujun Xu
fjxu@dhu.edu.cn

Baochun Wei
2140073@mail.dhu.edu.cn

Wei Liu
wliu@sues.edu.cn

Hongfei Zhu
477976285@qq.com

Yongyi Zhang
yyzhang2011@sinano.ac.cn

[1] Key Laboratory of High Performance Fibers & Products, Ministry of Education, Donghua University, Shanghai 201620, People's Republic of China

[2] College of Fashion Technology, Shanghai University of Engineering Science, Shanghai 201620, People's Republic of China

[3] Suzhou Institute of Nano-Tech and Nano-Bionics, No. 398 Ruoshui Road, Suzhou 215123, People's Republic of China

Introduction

Since the first well-recognized report of carbon nanotube (CNT) in 1991 [1], it has generated huge popularity in various areas due to their outstanding properties [2, 3]. CNT-reinforced composites can be used in various fields such as strain sensor, electrode in battery, gas detection, and so on [4–6]. The CNT composites exhibit excellent mechanical strength and other functional properties, such as high electrical conductivity, electrostatic shielding, and thermal stability [7]. However, the size of individual CNT is too small to be applied in industrial fields. Only CNT films should be the ideal candidate material for large-scale structures. Many methods can produce large-scale CNT film. For example, suspension-based vacuum filtration method [8–11], directly drawing method [12–14], floating catalyst chemical vapor deposition (FCCVD) method [15], and other methods including hydroentangling [16] and electrochemical chemical deposition [17]. However, the vacuum filtration method could not produce strong films [18]. Directly drawing method produces CNT films at high costs. Among these methods, the FCCVD is the most efficient way to produce large-scale CNT films with high quality at an acceptable cost [19]. FCCVD CNT film is one

of the most promising reinforcement materials for high performance composites.

Therefore, the in-plane mechanical properties and engineering constants of FCCVD CNT films are critical for the understanding of CNT film-based structures. In addition, the engineering constants are also important to the numerical simulation of CNT films [20]. The in-plane stress state of the two-dimensional CNT film can be analyzed via its compliance matrix ([S]) according to $[\varepsilon] = [S][\sigma]$ [21]. In the compliance matrix, four independent engineering constants, longitudinal Young's modulus (E_1), transverse Young's modulus (E_2), major Poisson's ratio (v_{12}), and in-plane shear modulus (E_s), govern the mechanical behavior of CNT films. Once these engineering constants are known, the mechanical behavior of CNT films would be determined. Although many works have been done to research the mechanical properties of CNT films. For example, Ma and coworkers reported the fabrication of FCCV D CNT films and analyzed its mechanical strength via Weibull theory [15]. Coleman and Blighe investigated the factors controlling the strength and modulus of CNT films [22]. Ting and Chang studied the influence of CNT conjunctions on the failure process of CNT films [23]. Recently, Pourhabib and Ding used finite element analysis to predict the modulus of buckypaper [24]. However, little paper researched the in-plane engineering constants of FCCVD CNT films.

In this study, we investigated the four independent in-plane engineering constants of FCCVD CNT films. The uniaxial tensile testing measured the longitudinal Young's modulus, transverse Young's modulus, Poisson's ratio, and in-plane shear modulus. The in-situ scanning electron microscopy (SEM) was conducted to observe the microstructures of CNT films during tensile test. Transmission electron microscopy (TEM) was adopted to observe the structure of individual CNT in the films. The reorientation of CNT bundles was analyzed via numerical image processing and Raman spectroscopy.

Experimental

FCCVD CNT films

The CNT films were received from the Suzhou Institute of Nano-Tech and Nano-Bionics (Suzhou, China). It was fabricated by FCCVD methods as shown in Fig. 1a. The ethanol, ferrocene, and thiophene were injected into the heated reactor (1300 °C) at a feeding rate of 0.15 ml min^{-1}. The Ar–H_2 mixture (volume ratio 1:1) was injected into the reactor at a rate of 4000 sccm. The aerogel-like carbon nanotubes grew spontaneously in the reactor, which can be blown out with the gas flow. The CNTs were wound onto the roller. During this process, the CNT bundles preferentially aligned to the take up direction. Thereafter, the porous CNT assemblies were densified by the ethanol. The as-prepared large-scale CNT films are shown in Fig. 1b.

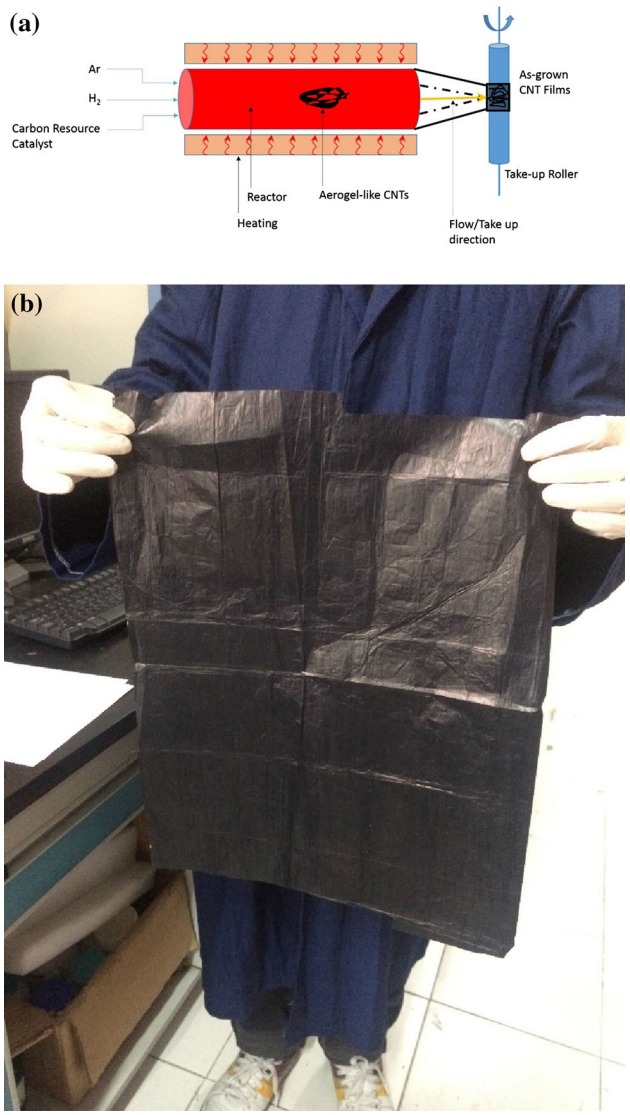

Fig. 1 **a** FCCVD fabrication process, **b** large-scale CNT films

Characterizations of CNT films

The purification of CNT film was determined via thermal gravity analyzer (TGA). The microstructures of CNT films were observed by the field emission SEM (FESEM, HITACHI S-4800). A specially designed SEM stage (Fig. 2a) was mounted in SEM chamber to observe the in-situ CNT deformation during tensile test. The thickness of CNT film was measured from the cross section (Fig. 2b)

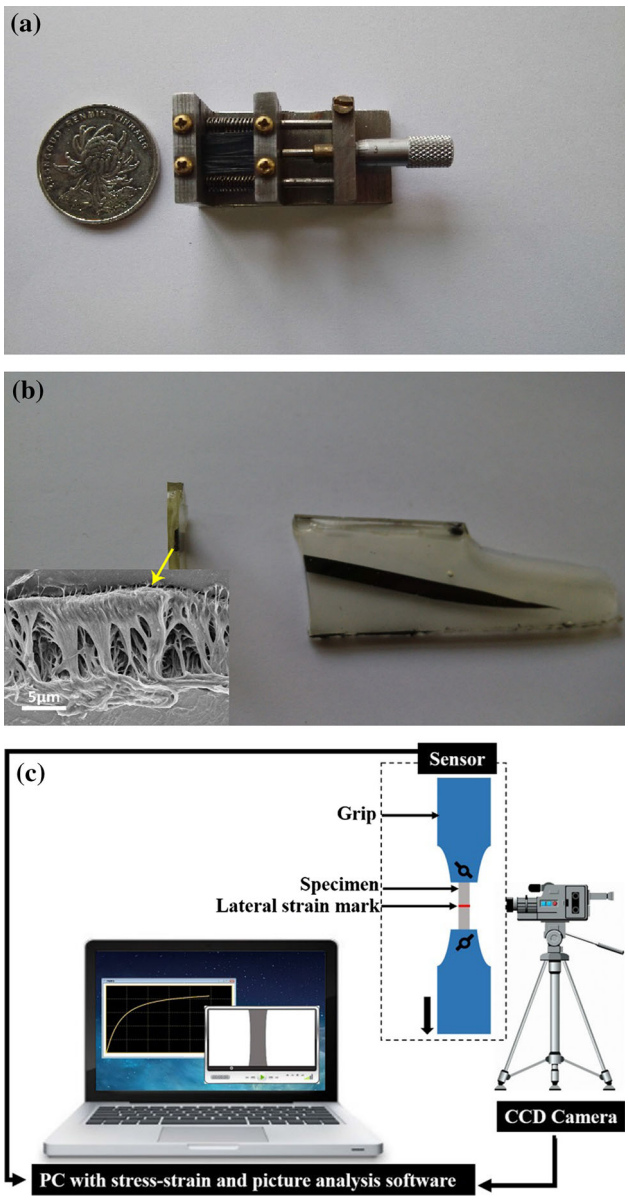

Fig. 2 **a** In-situ SEM testing stage, **b** brittle fracture surface, **c** schematic of uniaxial tensile and Poisson's ratio testing apparatus

under SEM. In addition, the nano-pore analyzer (Quantachrome Porometer 3 G-zh) was used to measure the pore distribution in the film. TEM (JEOL JEM-2100) was employed to observe the structure of individual CNT in the films. The numerical imaging processing method and Raman spectroscopy were adopted to analyze the reorientation of CNT bundles [25].

During the tensile testing, the tensile loads were applied onto specimen in three directions: (1) preferential/longitudinal direction, in which most of the CNT bundles aligned parallel to each other. This preferential alignment was caused by the material flow during fabrication as shown in Fig. 1a. The preferential direction was further defined as on-axis direction in the flowing, (2) transverse direction, which was perpendicular to the preferential direction, and (3) 45° off-axis direction. In addition, the gage length for tensile testing was 10 mm. The specimen width was 5 mm. All samples were tested on tensile tester (XS (08) XG, Fig. 2c). The extension rate was 0.3 mm min^{-1}. A camera was used to record the lateral strain simultaneously. At least 20 specimens were tested successfully for statistical analysis.

Results and discussions

Microstructures of CNT film

The TGA results in Fig. 3a demonstrated that the purification of CNT film was 87.7 %. The weight loss was the decomposition of catalyst and impurities in the film. As observed from TEM images (Fig. 3b), the CNT aggregated into bundles. The bundles entangled with each other and formed numerous contacts in CNT network as shown in Fig. 3c. The preferential alignment of CNT in the films is observed in Fig. 3c. Figure 3d shows the contact points between CNT bundles. It can be observed that two CNT bundles jointed into a big conjunction and formed Y-shape contact point. The length of the as-grown CNT-to-CNT contact was up to 250 nm, which was measured from the SEM images in Fig. 3d. This Y-shape conjunction spread out in the network and formed the freestanding CNT films via numerous contacts. This is quite different from that of vacuum filtration made buckypapers (BPs), in which the CNT bundles lay on each other and are held together by weak van der Waals forces only [22].

The thickness of the film was 10 ± 0.4 μm, which was measured from fracture surface as shown in Fig. 2b. The CNTs produced by FCCVD were MWCNT as shown in Fig. 3f. To determine the density of individual CNT (ρ_{CNT}), the weight was calculated by assuming the MWCNT to be a hollow cylinder with an 11 nm outer diameter, a 5 nm inner diameter, and a wall density of 2.1 g cm^{-3}, which equals to the density of graphite [26]. The inset picture in Fig. 3f illustrated this assumption. Therefore, the density of individual CNT can be calculated in Eq. (1) [27].

$$\rho_{CNT} = \frac{m}{V} = \frac{2.1 \times \pi(11^2 - 5^2)}{\pi \times 11^2} = 1.67 \quad (1)$$

In addition, Fig. 3e shows the pore distribution in CNT films. The Gaussian fitting demonstrated that the diameters of more than half of the pores ranging from 390 to 590 nm. Compared to the pore size in vacuum filtration made BPs, 10 μm [28], the FCCVD films had much smaller pore sizes, indicating more compact structure compared to BP. The

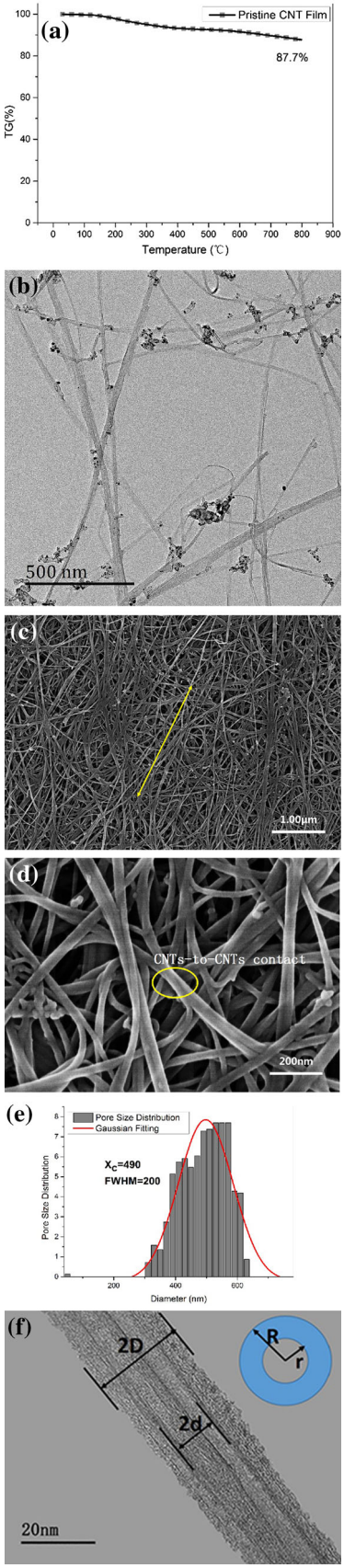

◀**Fig. 3** **a** TGA cure, **b** TEM image of CNTs, **c** FESEM image of CNT film under (*arrow* shows the preferential direction), **d** SEM images of the as-grown CNT-to-CNT contacts, **e** pore size and distribution, **f** TEM images of MWNTs

packing density (μ) was introduced to quantify the porosity of the films according to Eq. (2).

$$\mu = \frac{V_{\text{CNT}}}{V_{\text{total}}} = 1 - \frac{V_{\text{pore}}}{V_{\text{total}}} = \frac{\rho_{\text{film}}}{\rho_{\text{CNT}}}, \tag{2}$$

where V_{CNT}, V_{pore}, and V_{total} were the volumes occupied by CNTs, air, and the film, respectively. The density of CNT film (ρ_{film}) was measured to be 0.189 g cm^{-3}. Thus, packing density of CNT film was calculated to be 0.113, indicating the high porous structure of FCCVD films. This porous structure can provide enough space for resin filtration during composite fabrication.

Engineering constants of CNT films

Since a CNT film can be regarded as a 2D unidirectional material, the in-plane stress–strain relationship in longitudinal/on-axis direction can be determined by its compliance matrix in Eq. (3) [21].

$$\begin{bmatrix} \varepsilon_x \\ \varepsilon_y \\ \varepsilon_s \end{bmatrix} = \begin{bmatrix} \frac{1}{E_x} & -\frac{v_y}{E_y} & 0 \\ -\frac{v_x}{E_x} & \frac{1}{E_y} & 0 \\ 0 & 0 & \frac{1}{E_s} \end{bmatrix} \begin{bmatrix} \sigma_x \\ \sigma_y \\ \sigma_s \end{bmatrix} \tag{3}$$

The components with subscript in letter were engineering constants expressed under on-axis coordinate system as shown in Fig. 4. The on-axis direction represents the preferential direction in the films. Once the longitudinal Young's modulus (E_x), transverse Young's modulus (E_y), Poisson's ratio in longitudinal direction (v_x), transverse direction (v_y), and in-plane shear modulus (E_s) are known, the relationship between stress–strain can be determined.

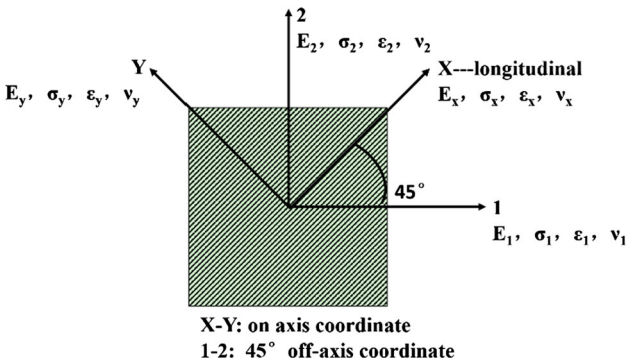

Fig. 4 Coordinates system

Among them, E_x, E_y, v_x, and v_y can be determined by uniaxial tensile testing. However, it is difficult to carry out the pure in-plane shear testing in the ultrathin CNT films. Therefore, E_s was calculated from the transformation relationship between the compliance under different coordinates system as illustrated in Fig. 4. The compliance of CNT films in 45° off-axis can be determined according to Eq. (4) [21].

$$\begin{bmatrix} \varepsilon_1 \\ \varepsilon_2 \\ \varepsilon_6 \end{bmatrix} = \begin{bmatrix} \frac{1}{E_1} & -\frac{v_{12}}{E_2} & \frac{v_{16}}{E_6} \\ -\frac{v_{21}}{E_1} & \frac{1}{E_2} & \frac{v_{26}}{E_6} \\ -\frac{v_{61}}{E_1} & \frac{v_{62}}{E_2} & \frac{1}{E_6} \end{bmatrix} \begin{bmatrix} \sigma_1 \\ \sigma_2 \\ \sigma_6 \end{bmatrix} \tag{4}$$

where components with subscripts in mathematica form correspond to the engineering constants under the 45° off-axis coordinate system as shown in Fig. 4. These parameters can be determined from the uniaxial tensile testing along the 45° off-axis direction. The transformation relationship between the compliance matrices under on-axis and 45° off-axis coordinate can be expressed as Eq. (5) [29].

$$\begin{bmatrix} \frac{1}{E_1} \\ \frac{1}{E_2} \\ -\frac{v_{12}}{E_2} \\ \frac{1}{E_6} \\ \frac{v_{16}}{E_6} \\ \frac{v_{26}}{E_6} \end{bmatrix} = \begin{bmatrix} \cos^4\theta & \sin^4\theta & 2\cos^2\theta\cdot\sin^2\theta & \cos^2\theta\cdot\sin^2\theta \\ \sin^4\theta & \cos^4\theta & 2\cos^2\theta\cdot\sin^2\theta & \cos^2\theta\cdot\sin^2\theta \\ \cos^2\theta\cdot\sin^2\theta & \cos^2\theta\cdot\sin^2\theta & \cos^4\theta+\sin^4\theta & -\cos^2\theta\cdot\sin^2\theta \\ 4\cos^2\theta\cdot\sin^2\theta & 4\cos^2\theta\cdot\sin^2\theta & -8\cos^2\theta\cdot\sin^2\theta & (\cos^2\theta-\sin^2\theta)^2 \\ 2\cos^3\theta\cdot\sin\theta & -2\cos\theta\cdot\sin^3\theta & 2(\cos\theta\cdot\sin^3\theta-\cos^3\theta\cdot\sin\theta) & \cos\theta\cdot\sin^3\theta-\cos^3\theta\cdot\sin\theta \\ 2\cos\theta\cdot\sin^3\theta & -2\cos^3\theta\cdot\sin\theta & 2(\cos^3\theta\cdot\sin\theta-\cos\theta\cdot\sin^3\theta) & \cos^3\theta\cdot\sin\theta-\cos\theta\cdot\sin^3\theta \end{bmatrix} \begin{bmatrix} \frac{1}{E_x} \\ \frac{1}{E_y} \\ -\frac{v_y}{E_y} \\ \frac{1}{E_6} \end{bmatrix} \tag{5}$$

Subsisting $\theta = 45°$ into Eq. (5), the in-plane shear modulus (E_s) can be calculated as Eq. (6).

$$\frac{1}{E_s} = \frac{4}{E_1} - \frac{1}{E_x} - \frac{1}{E_y} + \frac{v_y}{2E_y} \tag{6}$$

where E_1, E_x, and E_y were the modulus in 45° off-axis, preferential and transverse direction. v_y was Poisson's ratio in transverse direction. The uniaxial tensile tests were carried out in preferential/on-axis and 45° off-axis directions to determine these constants.

Modulus and tensile behavior

Figure 5 shows that the Young's modulus in longitudinal and transverse directions were 3 and 0.3 GPa, respectively. The highest tensile strength, 127 MPa, appeared in longitudinal direction. The strengths in transverse and 45-degree direction were 13 and 22 MPa, respectively. The poor CNT alignment in transverse direction led to the weakest strength. In 45-degree direction, the typical shear fracture surface (Fig. 6) indicated that the CNT bundles suffered from considerable shear force, which resulted in the poor tensile strength. In addition, the failure strain in longitudinal, 45-degree, and transverse direction were 26, 18, and 15 %, respectively. During the tensile process, more displacement was required to straighten the misaligned CNT bundles in transverse direction and 45-degree direction, rendering the larger tensile strains. This anisotropic mechanical property came from the preferential orientation of CNT bundles in the film as discussed previously.

Figure 7 [12, 16, 17, 22, 30–34] compares the mechanical properties of CNT films or BPs made by several different methods. It was obvious that FCCVD CNT films exhibited higher tensile strength and failure strain than the BPs. The tensile strength reported in this work was nearly two folds of the strongest BP and comparable to the state-of-art FCCVD films fabricated by Ma [30, 32]. The good mechanical property came from the as-grown CNT conjunctions between neighboring bundles as observed under SEM (Fig. 3d). As pointed out by Coleman et al. [22], the strength of CNT film was controlled by the adhesion force at CNT conjunctions. In FCCVD CNT films, the CNT bundles jointed together at the Y-shape conjunction, which grew up inherently during the

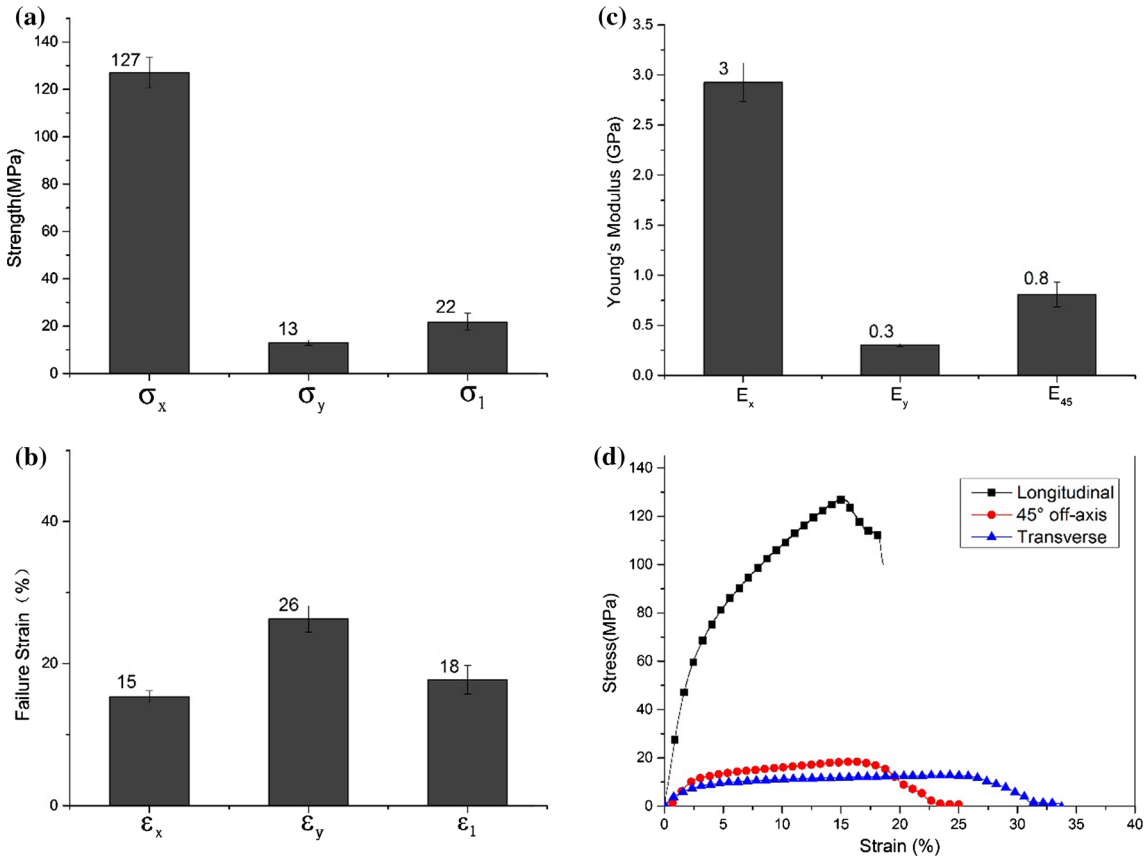

Fig. 5 **a** Tensile strength, **b** failure strain, **c** modulus, **d** typical stress–strain curves of CNT films in different directions

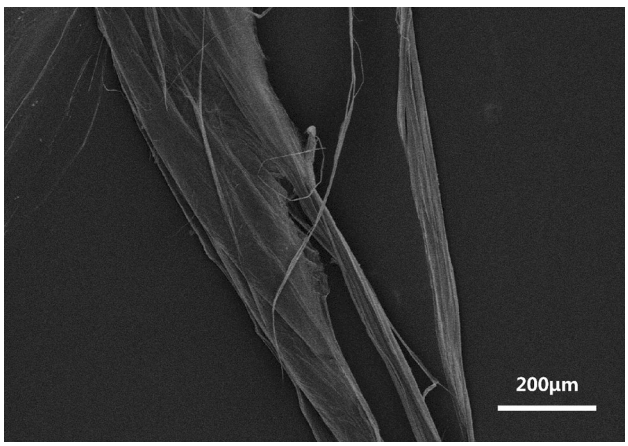

Fig. 6 SEM image of typical shear fracture surface in 45° direction

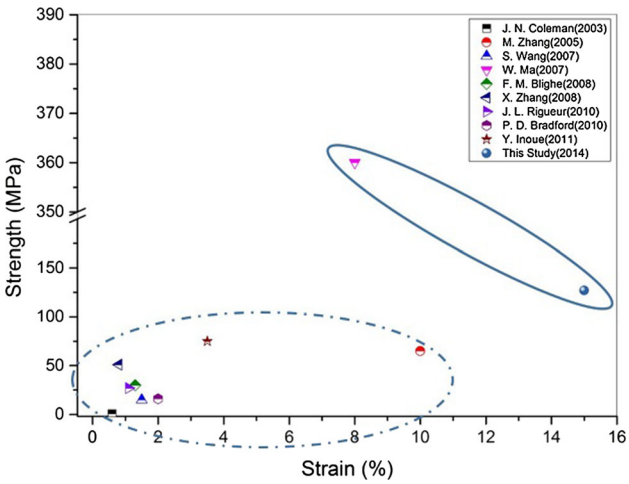

Fig. 7 Mechanical properties of FCCVD CNT films (*solid line* region) and buckypapers (*dash line* region)

fabrication process. Therefore, the FCCVD CNT films obtained higher adhesion force at CNT conjunctions, resulting in better mechanical property.

In addition, the CNT films showed similar viscoelastic tensile behavior as polymer did as shown in Fig. 5d. The Hookean elasticity phenomenon appeared at small strain and followed by the viscoelasticity behavior after the yield point [35]. Specifically, all the elastic engineering constants must be calculated under linear tensile behavior. The stress–strain curves of CNT films showed the linear tensile behavior before yield point. All parameters for determining the elastic engineering constants were measured from this linear region.

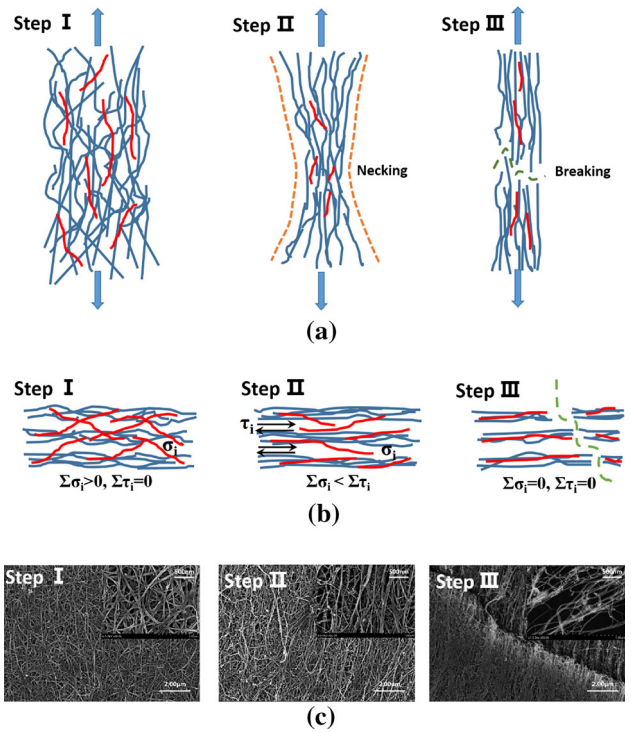

Fig. 8 Failure steps of CNT films **a** top view, **b** side view, **c** in-situ tensile observations

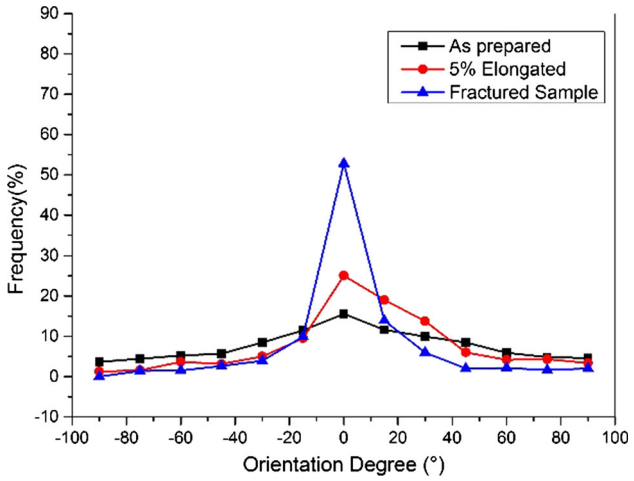

Fig. 9 Reorientation of CNT bundles simulated via numerical imaging process

The tensile behavior of CNT film was observed under in-situ SEM. At the first stage, the elongation of the curved and crimped CNT bundles led to the instant elastic behavior in CNT film as illustrated in step I in Fig. 8a. At the second stage, as shown in step two in Fig. 8a, the deformation of CNT bundles increased and the CNT-to-CNT contacts were to break. Consequently, the CNT bundles slipped from each other. The dissipation of friction energy in this process explained the plastic deformation of

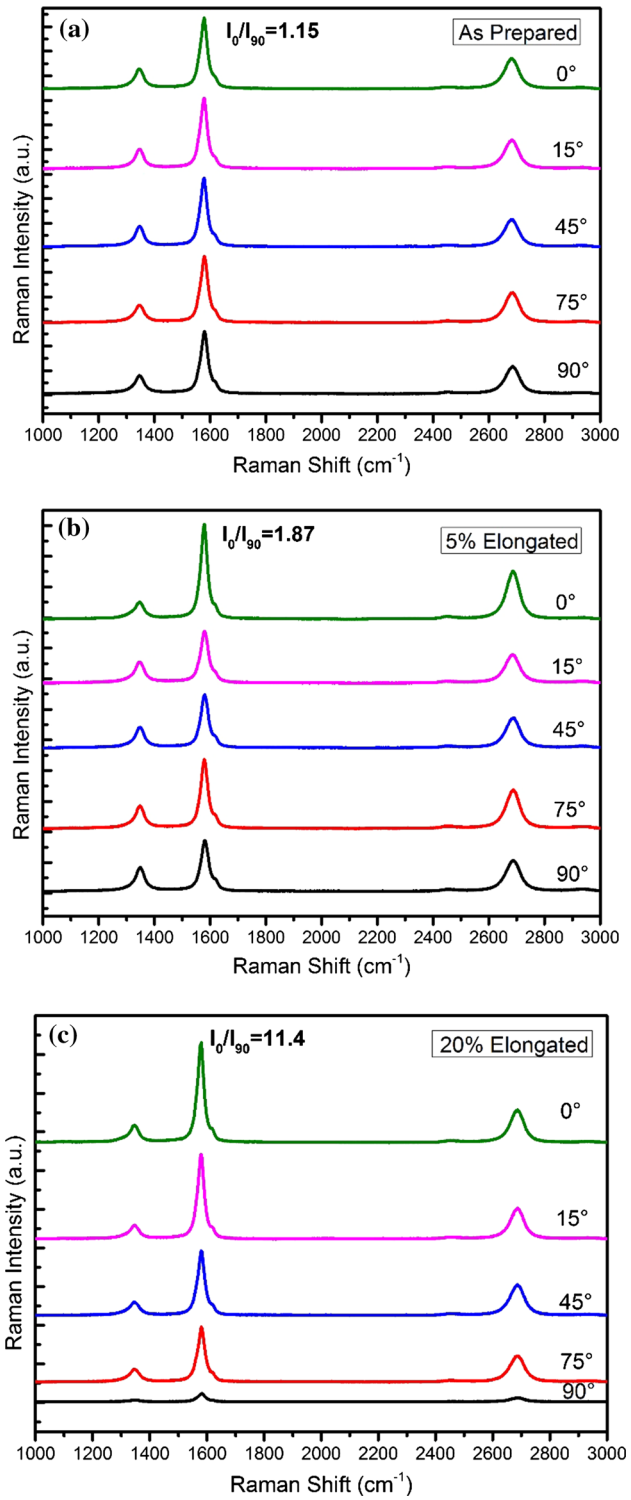

Fig. 10 Polarized Raman spectra of CNT film at 0 % strain (**a**), 5 % strain (**b**), and 20 % strain (**c**)

CNT film. Finally, inner CNT bundles pulled out from the network, resulting in the delamination in CNT films as shown in Fig. 8b. The CNT film broke up when the considerable CNT bundles had pulled out from the network.

Figure 8c shows the reorientation phenomenon of CNT bundles during tensile testing. Figure 9 concludes the orientation of CNT bundles at different tensile stages based on the numerical image analysis. It showed that only 15.6 % of CNT bundles preferentially aligned to the longitudinal direction at initial stage. When the sample was elongated by 5 %, more than 25 % CNT bundles aligned along this direction. This value increased to 52.8 % before the CNT films broke up. The redistribution of CNT bundles was consistent with the failure mechanism as discussed previously. In addition, the polarized Raman results as shown in Fig. 10 also supported the reorientation of CNT bundles. In polarized Raman spectroscopy, the G-band intensity of CNTs shows the maximum when the polarization is parallel to the stretched axis ($\psi = 0°$) and shows minimum at the perpendicular direction ($\psi = 90°$) [25], where ψ is the angle between polarization vector and stretched axis. Thus, the higher ratio of I_0/I_{90} would indicate better CNT alignment in stretched axis. The I_0/I_{90} were 1.15, 1.87, and 11.4, respectively, at 0, 5, and 20 % (near to fracture) strain, which demonstrated that more CNT bundles aligned to the stretched axis during tensile process.

Poisson's ratio

Poisson's ratios (PRs) in preferential direction and transverse direction were two essential parameters in Eq. (3). The testing results are shown in Table 1 and Fig. 11.

Table 1 PRs in different directions

Directions	Preferential direction (v_x)	Transverse direction (v_y)	45° off-axis direction (v_1)
PR at break	1.75	1.01	1.49
PR at 5 % strain	0.75	0.25	0.76

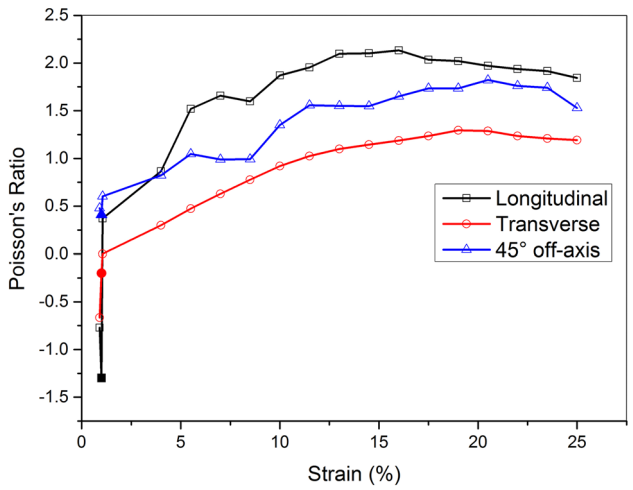

Fig. 11 Typical PR cures in different directions

Table 2 Parameters in compliance tensor for FCCVD CNT films

Parameters	E_x	E_y	v_x	v_y	E_s
Value	3 GPa	0.3 GPa	0.75	0.25	0.57 GPa

Figure 11 shows that all PRs increased gradually before 10 % strain and then leveled off until break. The increasing of PRs correlated to the reorientation of misaligned CNT bundles during tensile testing according to Fig. 8c. In addition, negative PRs were observed at 0.1 % strain in preferential direction and transverse direction, measured to be −0.99 and −0.55, respectively. Baughman, Fan, and Ma also observed the negative PR in CNT films [36–38]. The meandering CNTs in the films were pliable. The initial tensile load would elongate the wavy CNTs. Thus, the meandering CNTs would spread out under the in-plane load and expanded laterally, rendering the negative in-plane Poisson's ratio.

Shear modulus

Substituting E_1, E_x, E_y, and v_y into Eq. (6), the in-plane shear modulus was calculated to be 0.57 GPa. Due to the out of plane torsion force, it is difficult to carry out the pure in-plane shear testing for thin film in practice. We provided a more convenient way to calculate the in-shear modulus theoretically. By so far, all independent engineering constants in the compliance matrix of FCCVD CNT films are determined and shown in Table 2.

Conclusions

In this study, the in-plane mechanical properties and four engineering constants in compliance matrix of FCCVD CNT films were investigated. The Young's modulus and the Poisson's ratio in the compliance matrix were determined by the uniaxial tensile testing. The in-plane shear modulus was calculated to be 0.57 GPa based on the transformation between the compliance matrices of CNT films under different tensile loads. The tensile response of CNT bundles in the films was observed under in-situ SEM testing. The reorientation of CNT bundles was analyzed quantitatively via digital image processing method and Raman spectroscopy. The failure of CNT films was attributed to the slippage and pull out of CNT bundles.

Acknowledgements This work was supported by the National Natural Science Foundation of China (Grant No. 51303025), Shanghai Natural Science Foundation (Grant No. 12ZR1440500), Shanghai Science and Technology Committee (Grant No. 14YF1409600), and Specialized Research Fund for the Doctoral Program of Higher Education of China (Grant No. 20120075120016). This work was also

funded by Donghua University and the Fundamental Research Funds for the Central Universities. Thanks to Prof. Qingwen Li in Suzhou, Institute of Nano-tech and Nano-bionics, Chinese Academy of Sciences, for providing the FCCVD CNT material.

References

1. Iijima S (1991) Helical microtubules of graphitic carbon. Nature 354:56–58
2. De Volder MFL, Tawfick SH, Baughman RH, Hart AJ (2013) Carbon nanotubes: present and future commercial applications. Science 339:535–539
3. Jung Y, Kim T, Park CR (2015) Effect of polymer infiltration on structure and properties of carbon nanotube yarns. Carbon 88:60–69
4. Parikh K, Cattanach K, Rao R, Suh DS, Wu A, Manohar SK (2006) Flexible vapour sensors using single walled carbon nanotubes. Sens Actuators B 113:55–63
5. Wang Y, Yang Z, Hou Z, Xu D, Wei L, Kong ESW et al (2010) Flexible gas sensors with assembled carbon nanotube thin films for DMMP vapor detection. Sens Actuators B Chem 150:708–714
6. Li Z, Dharap P, Nagarajaiah S, Barrera EV, Kim JD (2004) Carbon nanotube film sensors. Adv Mater 16:640–643
7. Coleman JN, Khan U, Blau WJ, Gun'ko YK (2006) Small but strong: a review of the mechanical properties of carbon nanotube-polymer composites. Carbon 44:1624–1652
8. Rinzler A, Liu J, Dai H, Nikolaev P, Huffman C, Rodriguez-Macias F et al (1998) Large-scale purification of single-wall carbon nanotubes: process, product, and characterization. Appl Phys A Mater Sci Process 67:29–37
9. Jiang Q, Li Y, Xie J, Sun J, Hui D, Qiu Y (2013) Plasma functionalization of bucky paper and its composite with phenylethynyl-terminated polyimide. Compos B Eng 45:1275–1281
10. Jiang Q, Wang X, Zhu Y, Hui D, Qiu Y (2014) Mechanical, electrical and thermal properties of aligned carbon nanotube/polyimide composites. Compos B Eng 56:408–412
11. Oh JY, Yang SJ, Park JY, Kim T, Lee K, Kim YS et al (2014) Easy preparation of self-assembled high-density buckypaper with enhanced mechanical properties. Nano Lett 15:190–197
12. Zhang M, Fang S, Zakhidov AA, Lee SB, Aliev AE, Williams CD et al (2005) Materials science: strong, transparent, multifunctional, carbon nanotube sheets. Science 309:1215–1219
13. Liu W, Zhao H, Yong Z, Xu G, Wang X, Xu F et al (2013) Improving mechanical and electrical properties of oriented polymer-free multi-walled carbon nanotube paper by spraying while winding. Compos B Eng 53:342–346
14. Zhang L, Zhang G, Liu C, Fan S (2012) High-density carbon nanotube buckypapers with superior transport and mechanical properties. Nano Lett 12:4848–4852
15. Song L, Ci L, Lv L, Zhou Z, Yan X, Liu D et al (2004) Direct synthesis of a macroscale single-walled carbon nanotube nonwoven material. Adv Mater 16:1529–1534
16. Zhang X (2008) Hydroentangling: a novel approach to high-speed fabrication of carbon nanotube membranes. Adv Mater 20:4140–4144
17. Rigueur JL,Hasan SA, Mahajan SV, Dickerson JH (2010) Buckypaper fabrication by liberation of electrophoretically deposited carbon nanotubes. Carbon 48:4090–4099, 11
18. Nasibulin AG, Kaskela A, Mustonen K, Anisimov AS, Ruiz V, Kivistö S et al (2011) Multifunctional free-standing single-walled carbon nanotube films. ACS Nano 5:3214–3221
19. Liu L, Ma W, Zhang Z (2011) Macroscopic carbon nanotube assemblies: preparation, properties, and potential applications. Small 7:1504–1520
20. Gay D (2014) Mechanical behavior of laminated materials Composite materials: design and applications, 3rd edn. CRC press, Boca Raton
21. Kaw AK (2010) Macromechanical analysis of a lamina. In: Mechanics of composite materials, 2nd edn. CRC press, Boca Raton
22. Blighe FM, Lyons PE, De S, Blau WJ, Coleman JN (2008) On the factors controlling the mechanical properties of nanotube films. Carbon 46:41–47
23. Ting JM, Chang CC (2002) Multijunction carbon nanotube network. Appl Phys Lett 80:324–325
24. Pourhabib A, Huang JZ, Wang K, Zhang C, Wang B, Ding Y (2015) Modulus prediction of buckypaper based on multi-fidelity analysis involving latent variables. IIE Trans 47:141–152
25. Hwang J, Gommans H, Ugawa A, Tashiro H, Haggenmueller R, Winey KI et al (2000) Polarized spectroscopy of aligned single-wall carbon nanotubes. Phys Rev B 62:R13310
26. Lu Q, Keskar G, Ciocan R, Rao R, Mathur RB, Rao AM et al (2006) Determination of carbon nanotube density by gradient sedimentation. J Phys Chem B 110:24371–24376
27. Miao M (2011) Electrical conductivity of pure carbon nanotube yarns. Carbon 49:3755–3761
28. Špitalský Z, Aggelopoulos C, Tsoukleri G, Tsakiroglou C, Parthenios J, Georga S et al (2009) The effect of oxidation treatment on the properties of multi-walled carbon nanotube thin films. Mater Sci Eng B 165:135–138
29. Hahn HT, Tsai SW (1980) Off-axis stiffness of unidirectional composites in introduction to composite materials, vol 1. CRC Press, 109, p 65
30. Coleman JN, Blau WJ, Dalton AB, Muñoz E, Collins S, Kim BG et al (2003) Improving the mechanical properties of single-walled carbon nanotube sheets by intercalation of polymeric adhesives. Appl Phys Lett 82:1682–1684
31. Wang S, Liang Z, Wang B, Zhang C (2007) High-strength and multifunctional macroscopic fabric of single-walled carbon nanotubes. Adv Mater 19:1257–1261
32. Ma W, Song L, Yang R, Zhang T, Zhao Y, Sun L et al (2007) Directly synthesized strong, highly conducting, transparent single-walled carbon nanotube films. Nano Lett 7:2307–2311
33. Bradford PD, Wang X, Zhao H, Maria J-P, Jia Q, Zhu Y (2010) A novel approach to fabricate high volume fraction nanocomposites with long aligned carbon nanotubes. Compos Sci Technol 70:1980–1985
34. Inoue Y, Suzuki Y, Minami Y, Muramatsu J, Shimamura Y, Suzuki K et al (2011) Anisotropic carbon nanotube papers fabricated from multiwalled carbon nanotube webs. Carbon 49:2437–2443
35. Green MJ, Behabtu N, Pasquali M, Adams WW (2009) Nanotubes as polymers. Polymer 50:4979–4997
36. Baughman RH, Stafström S, Cui C, Dantas SO (1998) Materials with negative compressibilities in one or more dimensions. Science 279:1522–1524
37. Chen L, Liu C, Wang J, Zhang W, Hu C, Fan S (2009) Auxetic materials with large negative Poisson's ratios based on highly oriented carbon nanotube structures. Appl Phys Lett 94:253111
38. Ma YJ, Yao XF, Zheng QS, Yin YJ, Jiang DJ, Xu GH et al (2010) Carbon nanotube films change Poisson's ratios from negative to positive. Appl Phys Lett 97:061909